Soils and Rocks
An International Journal of Geotechnical and Geoenvironmental Engineering
www.soilsandrocks.com
ISSN 1980-9743
ISSN-e 2675-5475

Mechanical and numerical behavior of water jet-driven under-reamed concrete piles

Cesar Alberto Ruver[1#], Giovani Jordi Bruschi[1]

Article

Keywords
Under-reamed pile behavior
Finite element method (FEM)
Laboratory pile tests
Mini-cone tests
Numerical modelling
Water jet pile driving

Abstract

Water jet-driving technique has been shown as a viable practice for driving prefabricated piles in resistant soil layers. However, this technique is also associated with the reduction of load capacity of piles. Along these lines, the use of reams in prefabricated concrete piles improves their mechanical performance. The main objective of this research was to study the efficiency of reams on water jet-driven concrete piles; to this extent, pile loading tests and mini-cone tests were carried out before and after the driving of the piles. In addition, numerical modelling with the finite element method (*FEM*) was applied to study the stress-strain behavior. By means of the numerical modelling, it was possible to identify the stress and strain distribution at the tip, shaft, and reams of the piles; this allowed the understanding of the contribution of these elements in the total load capacity. Results have shown that the reams directly contribute for load capacity, with increases up to 40% when compared to conventional piles. Laboratory tests and numerical modeling proved to be fundamental tools to understand the mechanisms behind the contribution of reams to the load capacity of piles.

1. Introduction

Free fall hammers are traditionally utilized for the driving of prefabricated piles; international and national standards can be found with recommendations regarding the minimum weights of these hammers. The Brazilian standard for foundations (NBR 6122 - ABNT, 2019) indicates that for precast piles, hammers with a minimum weight of 40 kN should be utilized for workloads between 0.7 to 1.3 MN, in addition to a minimum weight of 75% of the pile weight. The aforementioned standard also refers to the maximum limits of compressive and tensile strength of the driving systems, considering the strength of the applied concrete. Sean Yoon (2014), recommends a minimum hammer weight of 12.5 kN, which should also be higher than a fourth of the pile weight. Wardani et al. (2020) state that, the hammer weight should be 50% of the pile weight plus a value of 6 kN. In this sense, if the hammer weight is not enough to surpass the strength of the soil, the specified foundation depth may not be reached or even structural damage to the piles may be evidenced. For such cases, the water jet-driving technique is recommended.

Although the water jet-driving technique is a consolidated practice in foundation engineering, several studies indicate that this driving method may compromise the strength of the soil, reducing its load capacity (Tsinker, 1988; Gunaratne et al., 1999; Mezzomo, 2009; Ruver et al., 2014; Passini, 2015; Moriyasu et al., 2016a, b). Mezzomo (2009) and Passini (2015) observed that, regardless the initial compaction degree (medium or dense) of the soil, the application of the water jet for pile driving results in a soil with a final loose state. Ruver et al. (2014), verified a load capacity loss between 53% and 90% in reduced models of concrete piles driven in fine sand, compared to the same models driven by percussion; authors also indicated that, higher flow rates also resulted in higher reductions in load capacity. Passini (2015) stated that the construction/operation procedures and the initial soil condition are factors that control the final load capacity of piles. Ruver & Jong (2019) verified that the initial compactness of the soil influences the load capacity of water jet-driven piles; nevertheless, the final soil state around the pile was the same for all cases.

Several authors have studied the effects of enlarged sections (i.e., reams) on the load capacity of piles, varying the number, position and shape (Mohan et al., 1969 ; Yabuuchi & Hirayama, 1993; Lee, 2007; Hirai et al., 2008; Honda et al., 2011; Choi et al., 2013; Qian et al., 2013; Christopher & Gopinath, 2016; George & Hari, 2015; Shetty et al., 2015;

[#]Corresponding author. E-mail address: cesar@ufrgs.br
[1]Universidade Federal do Rio Grande do Sul, Programa de Pós-Graduação em Engenharia Civil, Porto Alegre, RS, Brasil.

Submitted on December 2, 2022; Final Acceptance on April 1, 2023; Discussion open until August 31, 2023.
https://doi.org/10.28927/SR.2023.012822

Zarrabi & Esmali, 2016; Moayedi & Mosallanezhad, 2017; Vali et al., 2017; Zhang et al., 2018; Majumder & Chakraborty, 2022; Ziyara & Albusoda, 2022). In general, the insertion of reams improved the load capacity of the piles. Ruver (2013) evaluated the efficiency of a model of precast concrete pile with three reams driven by water jet, which presented more than twice the load capacity compared to the same pile without reams.

In order to better understand the bearing mechanism and contribution of the reams to the final load capacity of piles, several authors have been performing numerical modelling (Lee, 2007; Honda et al., 2011; George & Hari, 2015; Harris & Madabhushi, 2015; Moayedi & Mosallanezhad, 2017; Vali et al., 2017; Jong, 2019; Ruver & Jong, 2019; Ruver et al., 2019; Majumder & Chakraborty, 2022; Ziyara & Albusoda, 2022). In this context, the works of Jong (2019) and Ruver et al. (2019) demonstrated that, for short piles, two reams are sufficient, one placed at the toe and the other positioned in the intermediate portion of the shaft with a distance of three times the ream width, regardless of the ream thickness.

In this sense, the objective of this research was to evaluate the influence of reams on the bearing capacity of prefabricated concrete piles. To this extent, pile loading tests in reduced-scale were conducted; in such tests, optimized dimensions were utilized: (a) width/diameter of the reams were twice the width/diameter of the pile shaft; and (b) spacing between three width/diameter of the reams, plus two other configurations with a ream, at the toe or intermediate position of the shaft. FEM numerical modeling was applied to obtain the stress-strain behavior of the tests and determine the plastification strain zones of the soil, in addition to the normal stresses under the reams and shear stresses of the lateral faces of the piles. Penetrometric were carried out with a mechanical mini cone before and after driving the piles with a water jet to confirm the effect of strength loss in the area affected by the water jet.

2. Pile loading test (scaled-down)

The scale-down pile loading tests were conducted on precast square section piles with reduced dimensions, 0.50 m long and 0.05 cm on the shaft side, corresponding to 1:4 scale of a true size pile (0.20 m × 0.20 m cross-section). Four types of piles were studied (Figure 1): (a) without reams; (b) one ream at the toe (*T*); (c) one ream at the toe and one intermediate ream (*TI*); (d) one intermediate ream (*I*). The *TI* pile (a ream at the toe and another above the middle) is the model that presents the optimized geometry; it possesses a spacing of 0.30 m between the reams (3 times the ream width), as indicated by Qian et al. (2013), George & Hari (2015), Shetty et al. (2015), Jong (2019), and Ruver et al. (2019).

The tests were carried out in a stainless-steel tank of 0.7 m in diameter and 0.7 m in height. The tank was filled with a fine sand, from Osório town, south coast of Brazil,

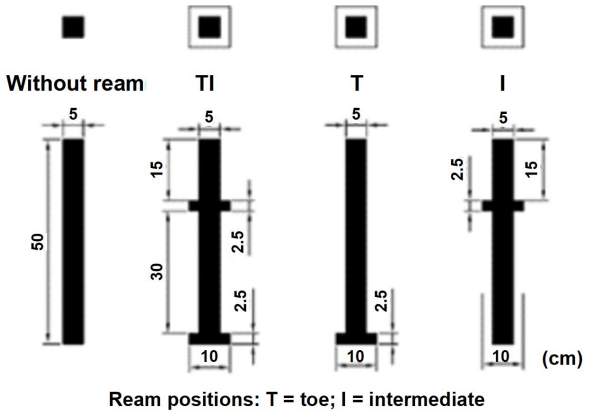

Figure 1. Tested piles models.

(ρ_s = 2.65 g/cm^3, e_{min} = 0.6 and e_{max} = 0.9). The sand was compacted in 10 cm layers with a manual wood socket, in the wet state (moisture content of 20%), and at a dry unit weight (ρ_d) of 1.559 g/cm^3 (equivalent to a compaction degree of 66.67%). After compacting the sand at the predetermined moisture content, the piles were inserted. First, two tests were carried out with piles without reams, one driven by percussion and the other by pressing, which served as reference for the loading capacity. The other piles were water jet-driven with a flow rate of 2.5 m^3/h and jet speed of 5.89 m/s. After the end of the driving procedure, the excess water was drained.

Before and after driving the piles, a mechanical mini-cone was inserted in the compacted soil. The mini-cone had a diameter of 7.9 mm with an inclination of 60º. The mini-cone was inserted at a constant speed of 3.5 mm/s. The driving strength was measured externally at the top of the rod, using a load cell with a capacity of 1 kN; considering that the reading of the applied load is external, it corresponds to the tip strength plus the skin friction of the soil. Before the driving of the piles, the mini-cone penetration was carried out in the center of the tank to evaluate the homogeneity of the compacted soil layers. After pile driving, the mini-cone peetratin was performed by water jet within the fluidized zone to identify and quantify the loss of soil strength.

The pile loading tests were conducted after pile driving and mini-cone penetration. The applied load was measured with a 20 kN (2,000 kgf) load cell. Displacements were measured using two 50 mm transducers, installed in opposite positions. For the load application, a 50 kN (5,000 kgf) hydraulic jack was used. The tests followed the procedures indicated by ASTM D 1143M (ASTM, 2020), in which the test is conducted with incremental load with each increment being 5% of the probable failure load, and maintained for 4 to 15 minutes each.

3. Numerical modelling

The Finite Element Method (FEM) with a 3D model was utilized for the numerical modelling. Piles and tank

dimensions are the same presented on section 2. For the fluidized zone, a prismatic zone surrounding the pile was considered with a width equal to twice the largest width of the piles, as indicated by Passini (2015). As for the boundary conditions, displacements in all three dimensions were prevented in the bottom ($\Delta x = \Delta y = \Delta z = 0$); while on the sides, only vertical displacements were allowed, preventing horizontal displacement ($\Delta x = \Delta y = 0$ and Δz = free), and the surface (top of the tank) was free.

Considering that the structural behavior was not the focus of this research, an linear-elastic constitutive model was attributed to the piles; with the elastic parameters estimated in accordance with the applied mortar. As for the soil, an elastic perfectly-plastic model was utilized, applying the Mohr-Coulomb failure criterion. The strength parameters for the soil were obtained in the work of Corte et al. (2017). A summary of the utilized parameters can be seen in Table 1.

The numerical modeling was divided into two steps: (a) application of the geostatic conditions; and (b) loading of the piles (total vertical displacement of 50 mm, applied in 50 increments). The displacement was applied at the top central node (master point), with the entire upper face linked to this node (slave surface), so that each applied displacement results in a reaction load at the same node. Steps of 1 second were adopted for the load application time, considering that the analysis was conducted as a drained condition. In the contact interfaces, two configurations were used: (a) rigid connection type (tie) (compacted and fluidized sand); and (b) friction interaction type (with roughness of 0.3) (penalty) and adherence (hard contact). The discretization of the mesh was made by rectangular elements of the structured type, with the central elements with 25 mm spacing between nodes. For the edge nodes, a spacing of 50 mm was adopted. As it is a three-dimensional modeling, elements composed of 8 nodes were used with reduced integration and processing time control. The average time for each modeling was 3 hours. Figure 2 shows the mesh discretization.

4. Results and discussion

Figure 3 presents the results of load versus settlement obtained in the numerical modeling, in comparison with the results of the laboratory tests carried out with the reduced models. Figure 4 shows a compilation of the results from numerical modeling. Up to a certain load, the numerical models converge with the results of the laboratory tests, at least up to settlements of of 7.5 mm failure criterion of ASTM D1143 (ASTM, 2020). For large loads (and settlements), some of the tested piles presented issues during testing (e.g., cracking of the reams); this behavior was not represented in the numerical modelling, considering that an elastic model was applied to the piles. Nonetheless, the behavior of the piles was fully represented up to the maximum levels of strain of ASTM D1143 (ASTM, 2020). Compared to the percussion-driven pile, the water jet-driven pile without reams presented a lower load capacity. On the other hand, the addition of reams recovered the lost bearing capacity and, in some cases, even increased it depending on the position and quantity of the reams (Figure 4).

Table 1. Numerical modelling parameters.

Material	ρ_{subm} (g/cm^3)	E (MPa)	ν	ϕ′ (º)	ψ (º)	c' (kPa)
Pile		20,000.0	0.2	-	-	-
Compacted soil	0.85	3.0	0.3	28	7.5	~2
Fluidized soil		1.8	0.3	20	0	~2

Legend: see List of Symbols.

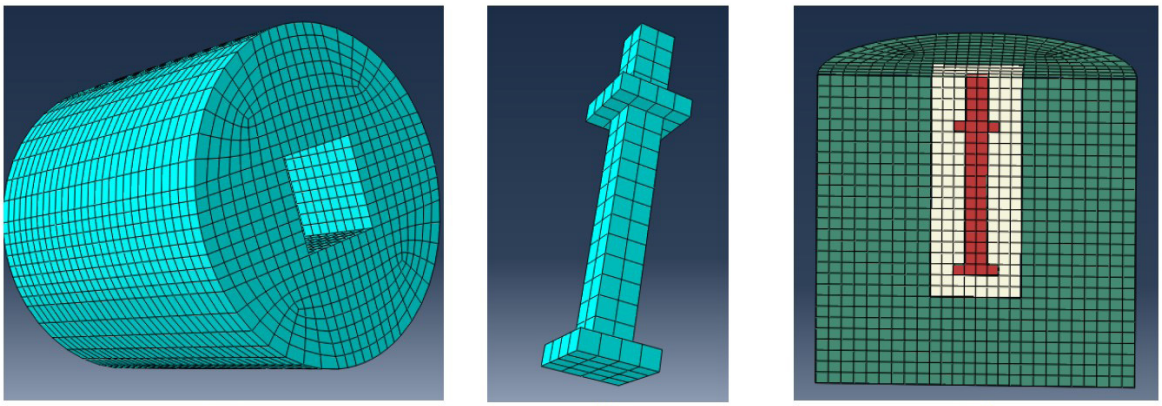

Figure 2. Mesh discretization: (a) compacted soil; (b) pile; (c) 3D model.

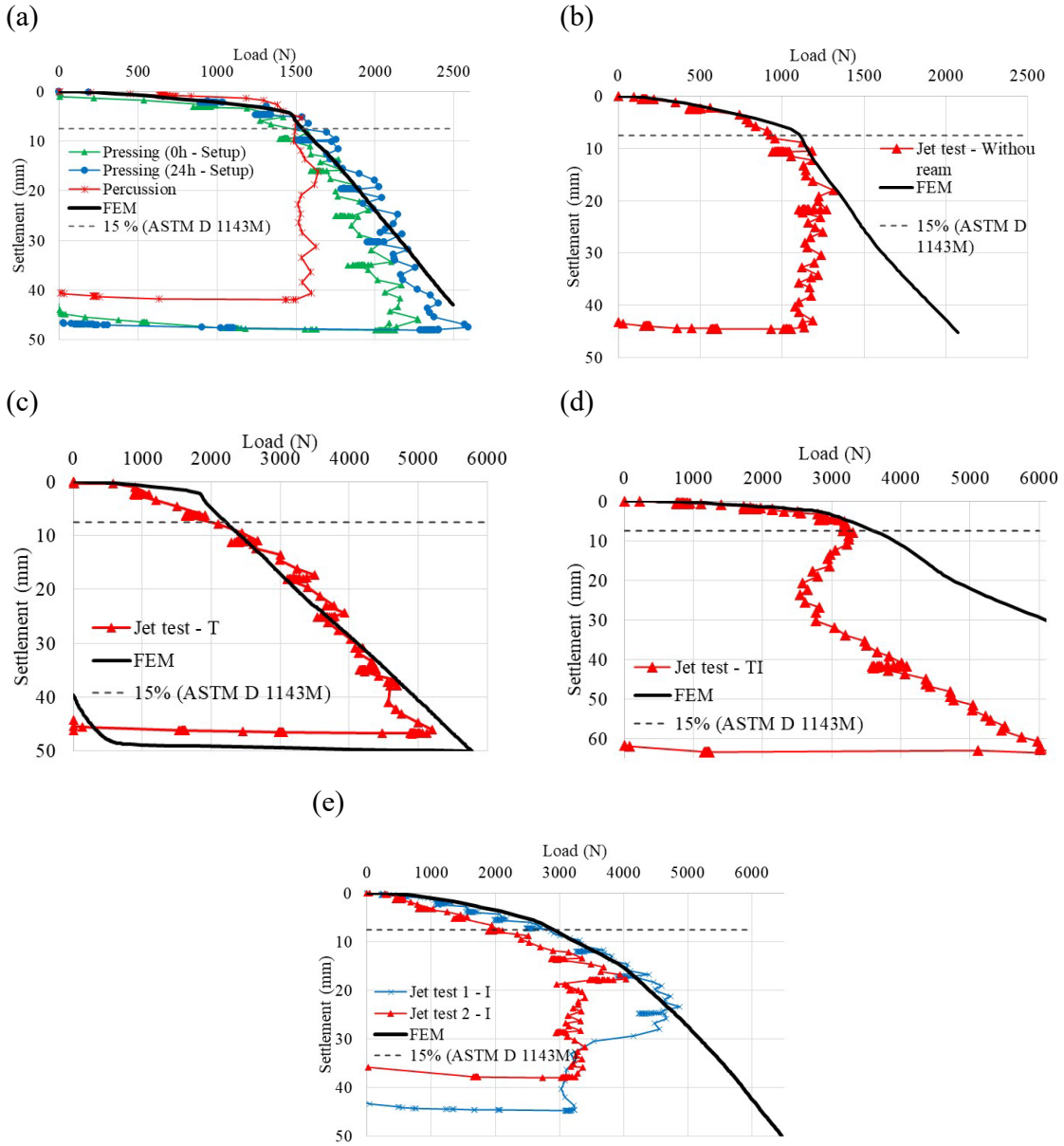

Figure 3. Comparison between laboratory and numerical results: (a) percussion drive – no ream; (b) water jet driven – no ream; (c) *T*; (d) *TI*; (e) *I*.

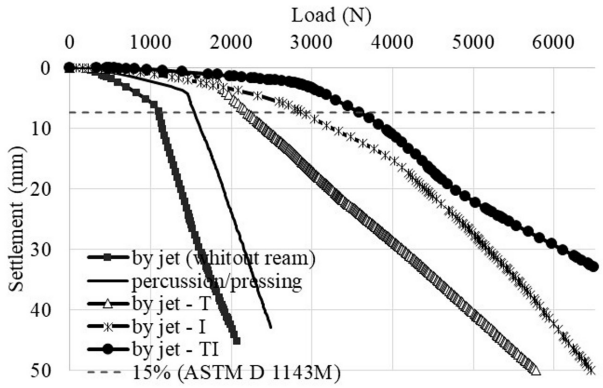

Figure 4. Numerical modeling for all tests.

The pile with two reams (*TI*) presented a better mechanical performance than both one-ream piles [i.e. toe (*T*) and intermediate (*I*)]. When comparing the one-ream piles, *T* piles resulted in a higher load capacity for small displacements, while *I* piles for great displacements. The same behavior was evidenced in the laboratory tests. The aforementioned behavior has also been attested by several studies (e.g., George & Hari (2015), Christopher & Gopinath (2016), Zarrabi & Esmali (2016)), in which two-reams piles result in a better mechanical performance when compared to one-ream ones.

Figure 5 shows the mini-cone results, before and after the driving of the piles. An increasing strength of linear

tendency was evidenced, indicating the homogeneity of the tested soil regarding its dry unit weight and compaction conditions. Also, it was possible to observe the deleterious effect of the water jet; represented by the reduction in strength of the mini-cone after the driving of the piles. Such an effect was more prominent in intermediate ream (*I)* piles, with strength losses up to 66%. The *I* piles presented the most execution/driving difficulties, considering that the water jet was concentrated at the tip and, consequently, was more concentrated near the shaft; thus, for the insertion of the widened portion, the fluidized region was narrower, causing more disturbance on the surroundings. The two-reams pile (*TI*) presented the lowest strength loss (50%); despite demanding a higher execution period, the disturbed region was wider, facilitating the introduction of the first (toe) and second (intermediate) reams, allowing better confinement of the soil between the reams. As for the *T* pile, the driving process was similar to the *TI* pile; however, as the disturbed region was larger due to the ream, less confinement was evidenced on the soil close to the shaft.

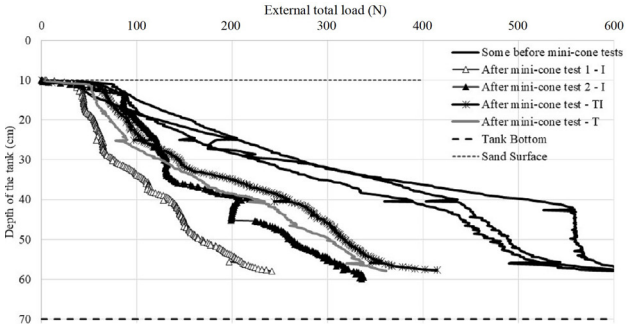

Figure 5. Mini-cone results.

Figure 6 presents the plastic strain results for settlements of 7.5 mm. For the *T* pile (Figure 6a), the plastic strain is concentrated along the lateral of the ream, with a larger strain area below the ream and smaller above it; also, a stress bulb was formed within the non-fluidized zone, while the other strains were concentrated within the fluidized zone. For large strains (settlements of 50 mm), the same behavior was evidenced, with the plastification zone advancing in the surroundings of the ream. As for the *I* pile (Figure 6b), plastic strains were verified along the ream and the tip for small settlements (7.5 mm), also presenting a larger strain area bellow the ream and smaller above it; for large settlements (50 mm) the same behavior was maintained, with plastic strains along the entire shaft advancing to the surface. Finally, for the *TI* pile (Figure 6c), the formation of a plastic zone within the fluidized zone was evidenced, covering the upper part of the intermediate ream, advancing vertically on the reams reaching the lower base from the ream of the base,

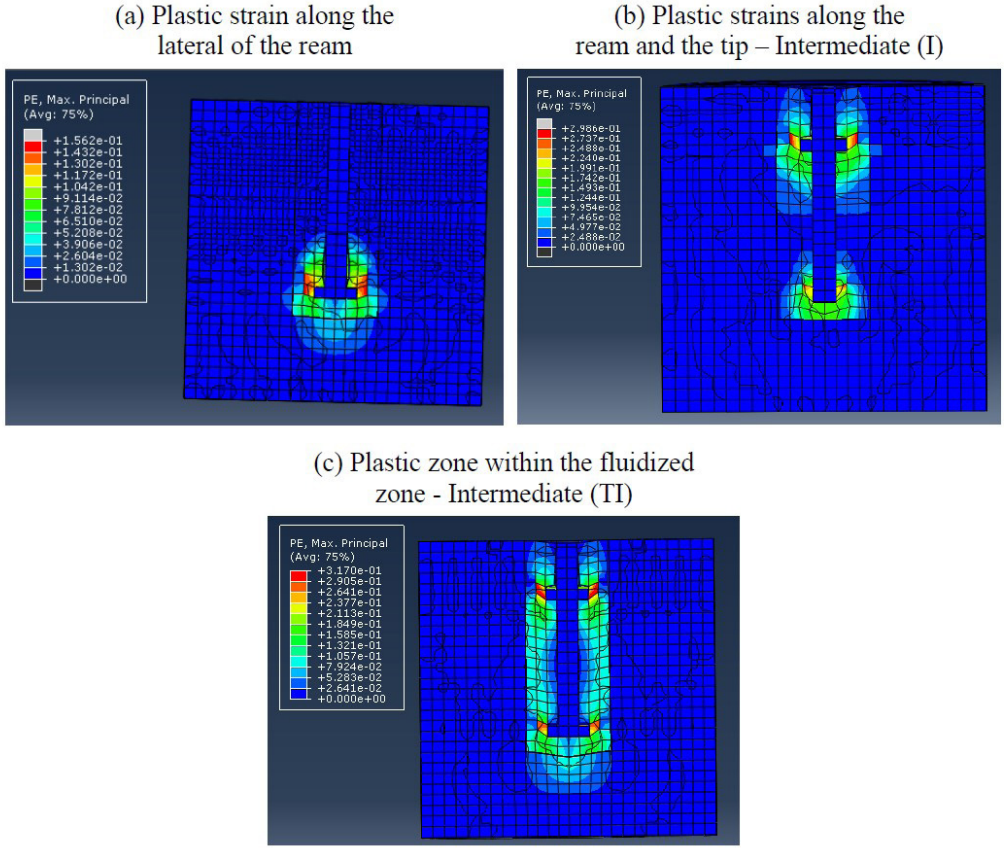

Figure 6. Plastic strains for settlements of 7.5 mm for the (a) T pile, (b) I pile, and (c) TI pile.

with no plastic strain on the soil between the reams. Also, for the pile with two reams (Figure 6c), there was the formation of a plastification zone reaching all the fluidized sand and the base bulb considerably invaded the non-fluidized sand.

Through numerical modeling it was possible to quantify the contribution of each of the components to the final load capacity. For uniform piles (continuous shaft), the load capacity is composed of lateral friction and tip strength. For reamed piles, the reams also contribute for strength generation, which in turn results in compressive loads on the soil. Figure 7a shows the distribution of compressive stresses under the reams and Figure 7b shows the distribution of lateral friction along the shaft and reams. Table 2 presents a compilation of the distribution of each of the portion of the total load capacity for a settlement of 7.5 mm.

Piles driven by conventional techniques presented a total load capacity of 1,576 N, while the one driven by water-jet presented a total load capacity of 1,127 N, which corresponds to a reduction of 28.5%. All three piles presented the same load contribution referring to tip and lateral friction (Figure 7b), with most of the load capacity being associated with tip contribution (>95%).

The toe ream pile (T), driven by water-jet, presented a total load capacity of 2,206 N; 40% higher than the percussion-driven pile and 96% higher than the water-driven pile with no ream (J). For the T pile, the tip strength corresponds to most of the load capacity contribution (>99.7%); this behavior is associated with the ream presence, preventing the confinement of the soil along the shaft and, consequently, the mobilization of lateral friction, as can be seen in Figure 7b.

For the intermediate ream pile (I*)*, the total load capacity was 2,862 N; 82% higher than the conventional piles (P/P). The intermediate ream was shown to be more efficient than the toe ream. In terms of ream contribution, 57.3% of the load capacity was attributed to the ream while 42.6% to the tip strength. The remaining load capacity was attributed to the shaft, being considered insignificant. Friction was only mobilized along the lateral faces of the ream (Figure 7b). For one ream piles (T or I), the tip strength is similar to water jet driven piles with no ream (J), indicating that the load capacity increase (57.3%) is related to the reams presence.

The two reams pile (TI) presented a total load capacity of 3.590 N; corresponding to more than 125% comparing to the reference pile (J/J) and more than triple the total load capacity of the water jet driven piles with no ream (J). Both reams presented similar contributions: 21.2% for the intermediate ream and 25.6% for the base ream. Together, the reams correspond to almost half of the mobilized load capacity. Analyzing Figure 7b, it is verified that the *TI* pile presents the highest lateral friction, which in turn reflects the highest value of total friction among the other piles.

The strength reduction of the soil (due to the fluidization process) was similar in all tests (Figure 5), while the increase in bearing capacity was attributed to the reams. The presence of one ream promoted a considerable increase in the bearing

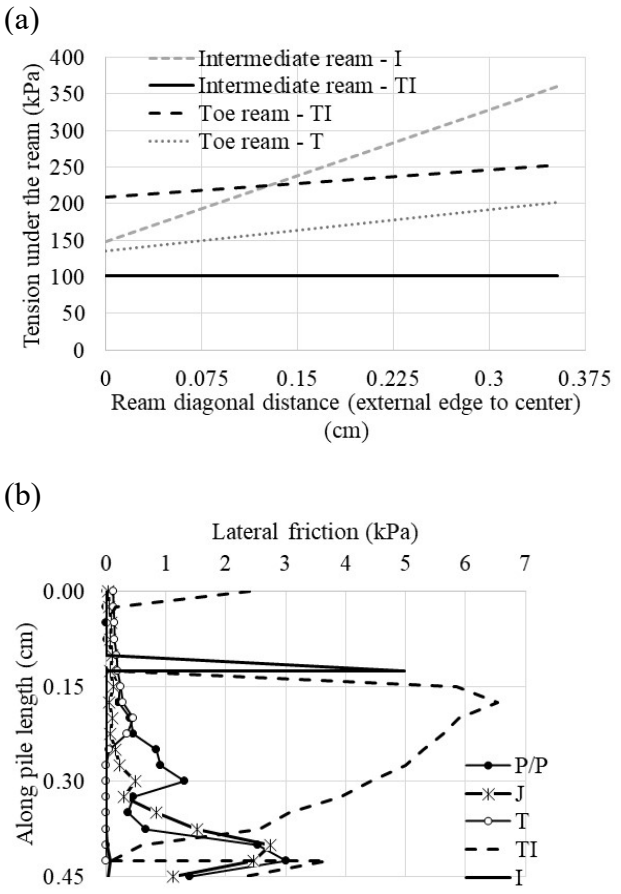

Figure 7. Stress distribution of (a) compression under of the ream, (b) shear (lateral friction) along the shaft and side of the reams for a 7.5 mm settlement.

Table 2. Load contribution of the elements for a settlement level of 7.5 mm.

Pile type	P/P		J		T		I		TI	
Load at 7.5 mm	N	%	N	%	N	%	N	%	N	%
Toe	1,514	96.1	1,077	95.6	936	42.4	1,220	42.6	1,720	47.9
Toe ream	-	-	-	-	1,265	57.3	-	-	920	25.6
Intermediate ream	-	-	-	-	-	-	1,641	57.3	760	21.2
Lateral friction	62	3.9	50	4.4	5	0.2	1	0.03	190	5.3
Total	1,576		1,127		2,206		2,862		3,590	

Legend: see List of Symbols.

capacity (96% to 218%), which in turn could be enhanced with the adequate positioning of this structural element. Although presenting a lower initial stiffness (Figure 4), the ream on the intermediate position resulted in a better mechanical performance when compared to the toe ream; with this behavior being attributed to the higher combined strength mobilization of the tip and the ream. For one-ream piles, current studies diverge on the best positioning of the ream, stating that different conditions (e.g., soil type, pile material, and ream shape) directly influence this behavior. Christopher & Gopinath (2016) state that, for metallic piles in sandy soil, toe reams result in the best mechanical behavior, in addition, regarding the ream positioning, the furthest from the tip, the lowest the bearing capacity of the pile. Ziyara & Albusoda (2022) studied piles driven in fine-grained soil, concluding that toe reams also result in the highest bearing capacity for saturated conditions; however, for unsaturated conditions, the best mechanical behavior is evidenced when the ream is more distant from the toe.

For piles with more than one ream, different studies have shown that the higher the number of reams, the higher the bearing capacity (considering a minimum distance so the reams can mobilize strength individually). For short piles, such as the case of this study, the bearing capacity was enhanced with two reams spaced three times the width of each ream. With that in mind, several studies also corroborate that the spacing of the reams is the most important factor for strength mobilization, alongside with ream number (Qian et al., 2013; George & Hari, 2015; Shetty et al., 2015; Moayedi & Mosallanezhad, 2017; Jong, 2019; Ruver et al., 2019).

5. Conclusions

The present research evaluated the influence of reams on the bearing capacity of prefabricated piles, both experimentally and numerically. Based on the findings of this research, the following conclusions can be disclosed:

a) The utilization of prefabricated piles with enlarged sections – reams, not only recovers the load capacity lost by the deleterious effect of the water jet but also results in a load capacity superior to a pile of uniform section driven by percussion.
b) Carrying out pile loading tests with reduced models in the laboratory, combined with the use of the mini-cone test before and after driving the piles, was essential to understand the bearing mechanism of the reams and the loose of load capacity effect by water-jet;
c) The adopted numerical modeling proved to be efficient, as it was able to reproduce the stress-strain behavior of the load tests with the reduced models up to the failure criterion indicated by ASTM (2020);
d) Through the numerical modeling it was possible to obtain the plastic deformation diagrams of the soil and the normal and shear stresses that act along all the faces of the piles. These elements were of fundamental importance, as they allowed understanding the bearing mechanism of the reams, as well as the estimation of the load contribution of each element in the total load capacity of the piles.

Declaration of interest

The authors have no conflicts of interest to declare. All co-authors have observed and affirmed the contents of the paper and there is no financial interest to report.

Authors' contributions

Cesar Alberto Ruver: Conceptualization, Methodology, Data curation, Visualization, Writing, Editing – original draft. Giovani Jordi Bruschi: data analyzing, writing, reviewing, editing.

Data availability

The datasets generated analyzed in the course of the current study are available from the corresponding author upon request.

List of symbols

c'	effective cohesive intercept
e_{max}	maximum void ratio
e_{min}	minimun void ratio
E	elasticity modulus
I	intermediate ream position
J	jet water driven of pile without under ream
P/P	percussion and pressing driven
T	toe ream position
TI	toe and toe reams positions
ϕ'	effective friction angle
ν	*Poison* coefficient
ρ_d	specific mass of dry soil
ρ_s	specific mass of solids
ρ_{subm}	specific mass of submerged soil
ψ	dilatancy

References

ABNT NBR 6122. (2019). *Design and construction of foundations*. ABNT - Associação Brasileira de Normas Técnicas, Rio de Janeiro, RJ (in Portuguese).

ASTM D1143. (2020). *Standard test methods for deep foundation elements under static axial compressive load*. ASTM International, West Conshohocken, PA. https://doi.org/10.1520/D1143_D1143M-20.

Choi, Y., Kim, D., Kim, S., Nam, M.S., & Kim, T. (2013). Implementation of noise-free and vibration-free PHC screw piles on the basis of full-scale tests. *Journal of Construction Engineering and Management*, 139(8),

960-967. http://dx.doi.org/10.1061/(ASCE)CO.1943-7862.0000667.

Christopher, T., & Gopinath, B. (2016). Parametric study of under-reamed piles in sand. *International Journal of Engineering Research & Technology (Ahmedabad)*, 5(7), 577-581. http://dx.doi.org/10.17577/IJERTV5IS070450.

Corte, M.B., Festugato, L., & Consoli, N.C. (2017). Development of a cyclic simple shear apparatus. *Soils and Rocks*, 40(3), 279-289. http://dx.doi.org/10.28927/SR.403279.

George, B.E., & Hari, G. (2015). Numerical investigation of under reamed pile. In *6th International Geotechnical Symposium*, Chennai, India. Retrieved in December 2, 2022, from https://igschennai.in/IGC2016_IIT_Madras/igc2016proceedings/papers/THEME2/IGC_2016_paper_487.pdf

Gunaratne, M., Hameed, R.A., Kuo, C., Reddy, D.V., & Patchu, S. (1999). *Investigation of the effects of pile jetting and preforming* (Technical Repport N. 772). Florida Department of Transportation.

Harris, D. E., Madabhushi, G. S. P. (2015). Uplift capacity of an under-reamed pile foundation. *Proceedings of the Institution of Civil Engineers - Geotechnical Engineering*, 168(6), 526-538. https://doi.org/10.1680/jgeen.14.00154.

Hirai, Y., Wakai, S., & Aoki, M. (2008). Development of multi-belled cast-in-place concrete pile construction method. *Journal of Technology and Design*, 14(28), 433-438. http://dx.doi.org/10.3130/aijt.14.433.

Honda, T., Hirai, Y., & Sato, E. (2011). Uplift capacity on balled and multi-belled piles in dense sand. *Soil and Foundation*, 51(3), 483-496. http://dx.doi.org/10.3208/sandf.51.483.

Jong, G.V.D. (2019). *Modelagem numérica do comportamento de estacas nervuradas cravadas por jato de água* [Undergraduate thesis, Federal University of Rio Grande do Sul]. Federal University of Rio Grande do Sul's repository (in Portuguese). Retrieved in December 2, 2022, from http://hdl.handle.net/10183/200223.

Lee, C.Y. (2007). Settlement and load distribution analysis of underreamed piles. *Journal of Engineering and Applied Sciences (Asian Research Publishing Network)*, 2(4), 36-40.

Majumder, M., & Chakraborty, D. (2022). Bearing capacity of under-reamed piles in clay using lower bound finite element limit analysis. *International Journal of Geotechnical Engineering*, 16(9), 1104-1115. http://dx.doi.org/10.1080/19386362.2022.2044102.

Mezzomo, S.M. (2009). *Study of the fluidisation mechanism in sandy soils using water jets* [Master's dissertation, Federal University of Rio Grande do Sul]. Federal University of Rio Grande do Sul's repository (in Portuguese). Retrieved in December 2, 2022, from http://hdl.handle.net/10183/23970.

Moayedi, H., & Mosallanezhad, M. (2017). Uplift resistance of belled and multi-belled piles in loose sand. *Measurement*, 190, 346-353. http://dx.doi.org/10.1016/j.measurement.2017.06.001.

Mohan, D., Murthy, V.N.S., & Jain, G.S. (1969). Design and construction of multi-underreamed piles. In *7th International Conference of Soil Mechanics and Foundation Engineering* (Vol. 2, pp. 183-186). Mexico: Sociedad Mexicana de Mecanica.

Moriyasu, S., Ishihama, Y., Takeno, T., Taenaka, S., Kubota, K., Tanaka, R., Nishiumi, K., & Harata, N. (2016a). Development of new-type steel-pile method for port facilities. In *Nippon Steel & Sumitomo Metal Technical Report* (pp. 50-56). Tokyo: Nippon Steel.

Moriyasu, S., Morikawa, Y., Yamashita, H., & Taenaka, S. (2016b). Evaluation of the vertical bearing capacity of steel pipe piles driven by the vibratory hammer Method with water and cement milk jetting. In *15th Asian Regional Conference on Soil Mechanics and Geotechnical Engineering* (pp. 1291-1295). Tokyo: Japanese Geotechnical Society Special Publication. https://doi.org/10.3208/jgssp.JPN-126.

Passini, L.B. (2015). *Installation and axial load capacity of fluidized model piles in sandy soils* [Master's dissertation, Federal University of Rio Grande do Sul]. Federal University of Rio Grande do Sul's repository (in Portuguese). Retrieved in December 2, 2022, from http://hdl.handle.net/10183/131011.

Qian, Y., Xu, G., Wang, R. (2013). Experimental research on failure behavior of soil around pile under compression. *Indonesian Journal of Electrical Engineering and Computer Science*, 11(4), 2013-2017. http://dx.doi.org/10.11591/telkomnika.v11i4.2377.

Ruver, C.A. (2013). *Estudo do comportamento de estacas pré-fabricadas cravadas por jato de água (research report)*. Rio Grande: FURG. (in Portuguese).

Ruver, C.A., & Jong, G.V.D. (2019). Estacas nervuradas cravadas por jato de água: análise paramétrica da influência da compacidade. In *X Seminário de Engenharia Geotécnica do Rio Grande do Sul* (pp. 1-9). São Paulo: ABMS. (in Portuguese).

Ruver, C.A., Ferronato, B., Dalla Vecchia, D., Spaniol, E.M.R., Silva, G.G., & Palomino, J.M.V. (2014). Comparação entre cravação por percussão e jato de água. In *XVII Congresso Brasileiro de Mecânica dos Solos e Engenharia Geotécnica* (pp. 1-10). São Paulo: ABMS. (in Portuguese)

Ruver, C.A., Jong, G.V.D., & Peres, M.S. (2019). Modelagem numérica do comportamento de estacas nervuradas cravadas por jato de água. In *XII Simpósio de Práticas de Engenharia Geotécnica da Região Sul* (pp. 1-10). Joinville: UFSC (in Portuguese).

Sean Yoon, P.E. (2014). *Pile driving best practice* (TxDOT Bridge Presentations Webinar). Texas Department of Transportation.

Shetty, P., Naveen, B.S., & Naveen, K.B.S. (2015). Analytical study on geometrical features of under-reamed pile by

Ansys. *International Journal of Modern Chemistry and Applied Science*, 2(3), 174-180.

Tsinker, G. (1988). Pile jetting. *Journal of Geotechnical Engineering*, 114(3), 326-334.

Vali, R., Khotbehsara, E.M., Saberian, M., Li, J., Mehrinejad, M., & Jahandari, S. (2017). A three-dimensional numerical comparison of bearing capacity and settlement of tapered and under-reamed piles. *International Journal of Geotechnical Engineering*, 13(3), 236-248. http://dx.doi.org/10.1080/19386362.2017.1336586.

Wardani, M.K., Aulady, M.F.N., Frido, W., & Handri, S. (2020). Determining the weight of the hammer based on expert experience for estimating load-carrying capacity. *IOP Conference Series. Materials Science and Engineering*, 1010, 012041. Retrieved in December 2, 2022, from https://iopscience.iop.org/article/10.1088/1757-899X/1010/1/012041/pdf

Yabuuchi, S., & Hirayama, H. (1993). Bearing mechanisms of nodal piles in sand. In W.F. Van Impe & P.O. Van Impe (Eds.), *Deep foundations on bored and auger piles* (pp. 333-336). Balkema.

Zarrabi, M., & Esmali, A. (2016). Behavior of piles under different installation effects by physical modeling. *International Journal of Geomechanics*, 16(5), 04016014. http://dx.doi.org/10.1061/(ASCE)GM.1943-5622.0000643.

Zhang, L., Chen, Q., Gao, G., Ninbalkar, S., & Chiaro, G. (2018). A new failure load criterion for large-Diameter under-reamed piles: practical perspective. *International Journal of Geosynthetics and Ground Engineering*, 4(3), 1-9. http://dx.doi.org/10.1007%2Fs40891-017-0120-8

Ziyara, H.M., & Albusoda, B.S. (2022). Experimental and numerical study of the bulb's location effect on the behavior of under-reamed pile in expansive soil. *Journal of the Mechanical Behavior of Materials*, 31(1), 90-97. http://dx.doi.org/10.1515/jmbm-2022-0010.